Electron-impact ionization of Fe^{14+} and other atomic ions in the Mg isoelectronic sequence

D.M. Mitnik [a], J.A. Shaw [a], M.S. Pindzola [a], D.C. Griffin [b], N.R. Badnell [c]

[a] *Department of Physics, Auburn University, Auburn, AL 36849, USA*
[b] *Department of Physics, Rollins College, Winter Park, FL 32789, USA*
[c] *Department of Physics and Applied Physics, University of Strathclyde, Glasgow G4 0NG, UK*

Abstract

Distorted-wave calculations are carried out for the electron-impact ionization of Fe^{14+} in both the ground $3s^2\ ^1S_0$ and metastable $3s3p\ ^3P_{0,2}$ levels. The cross sections and Maxwellian-averaged rate coefficients include direct ionization of the $2s$, $2p$, $3s$, and $3p$ subshells, as well as inner-shell excitations from the $2s$ and $2p$ subshells leading to autoionization. The excitation–autoionization contributions are found to be large for both the ground and metastable levels. To assist modeling efforts of moderately dense plasmas, the direct and indirect rate coefficients are resolved as to the final level of the ionization process and assembled in a standard database file. A complete database for selected metallic ions in the Mg isoelectronic sequence will reside in electronic form at the Controlled Fusion Atomic Data Center at ORNL (http://www-cfadc.phy.ornl.gov/data_and_codes/). © 1998 Elsevier Science B.V.

1. Introduction

Like their counterparts in the Na isoelectronic sequence [1], atomic ions in the Mg isoelectronic sequence have been predicted [2–5] to show strong excitation–autoionization (EA) enhancements in their total electron-impact ionization cross sections. Experimental efforts [6], however, for the Mg-like ions have been clouded by the possible presence of unknown fractions of metastable states in the ion beam. In fact, no experimental measurements have been made for atomic ions with higher charge states than Ar^{6+}. Thus, efforts to model transition metal ions in moderately dense plasmas [7] must currently rely on theoretical calculations of electron-impact ionization rate coefficients.

In this paper we carry out multiconfiguration intermediate-coupled distorted-wave calculations for the electron-impact ionization of Fe^{14+} in both the ground $3s^2\ ^1S_0$ and metastable $3s3p\ ^3P_{0,2}$ levels. The cross sections include direct ionization of the $2s$, $2p$, $3s$, and $3p$ subshells, as well as inner-shell excitations from the $2s$ and $2p$ subshells leading to autoionization. The present calculations are more accurate than the previously reported [8] statistically-partitioned configuration-average ionization cross sections. The results will provide guidance for experimental efforts at measuring the ground and metastable cross sections separately. Although

most ionization experiments count charge changing events and thus sum over all final levels of the ionization process, the modeling of moderately dense plasmas requires final level resolved ionization cross sections and rate coefficients. To assist modeling efforts, we provide direct and indirect Maxwellian-averaged rate coefficients for Fe^{14+} resolved as to the final level of the ionization process and assembled in a standard database file. A complete database for the Ti, Cr, Fe, and Ni ions in the Mg isoelectronic sequence will reside in electronic form at the Controlled Fusion Atomic Data Center at ORNL. In the following sections we first review distorted-wave theory as applied to the electron-impact ionization of atomic ions in Section 2 and then present our cross section and rate coefficient results for Fe^{14+} in Section 3. A brief summary is found in Section 4.

2. Theory

Major contributions to the electron-impact single-ionization cross section are made by the following two processes:

$$e^- + A^{q+} \rightarrow A^{(q+1)+} + e^- + e^- , \tag{1}$$

and

$$e^- + A^{q+} \rightarrow (A^{q+})^* + e^- \rightarrow A^{(q+1)+} + e^- + e^- , \tag{2}$$

where A represents an arbitrary ion with charge q. The first process is direct ionization while the second is excitation–autoionization. Assuming the two processes occur independently and do not interfere, the total ionization cross section is given by

$$\sigma_T(g \rightarrow f) = \sigma_{DI}(g \rightarrow f) + \sigma_{EA}(g \rightarrow f) , \tag{3}$$

where $\sigma_{DI}(g \rightarrow f)$ is the direct ionization cross section and $\sigma_{EA}(g \rightarrow f)$ is the excitation–autoionization cross section from an initial level g of the N-electron ion to a final level f of the $(N-1)$-electron ion. The excitation–autoionization cross section through inner-shell excitation to an intermediate autoionizing level j is given by

$$\sigma_{EA}(g \rightarrow f) = \sum_j \sigma_E(g \rightarrow j) \left[\frac{A_a(j \rightarrow f) + \sum_i A_r(j \rightarrow i) B_a(i \rightarrow f)}{\sum_k A_a(j \rightarrow k) + \sum_i A_r(j \rightarrow i)} \right]$$

$$\equiv \sum_j \sigma_E(g \rightarrow j) B_a(j \rightarrow f) , \tag{4}$$

where $\sigma_E(g \rightarrow j)$ is the excitation cross section from level g to level j, $A_a(j \rightarrow k)$ is the autoionizing rate from level j to level k, $A_r(j \rightarrow i)$ is the radiative rate from level j to any lower energy level i, and $B_a(j \rightarrow f)$ is the multiple or effective branching ratio for autoionization from level j to level f, defined by the term in large square brackets. This term contains in turn the effective branching ratio $B_a(i \rightarrow f)$ for further (secondary) autoionization from level i to level f. Thus the effective autoionization branching ratios are defined by the recursive expression

$$B_a(i \rightarrow f) \equiv \left[\frac{A_a(i \rightarrow f) + \sum_{n<i} A_r(i \rightarrow n) B_a(n \rightarrow f)}{\sum_k A_a(i \rightarrow k) + \sum_{n<i} A_r(i \rightarrow n)} \right] . \tag{5}$$

This allows one to take into account all the possible secondary autoionizations following cascading, until the radiative decay reaches a level m below the first ionization limit such that $B_a(m \rightarrow f) = 0$.

A theoretical calculation of the total electron-impact ionization cross section for an arbitrary ion divides into three parts. The first part is a collisional ionization calculation for σ_{DI}, the second part is a collisional excitation

calculation for σ_E, and the third part is an atomic structure calculation for B_a. The Maxwellian rate coefficients for an atomic database are then separately calculated and catalogued for σ_{DI} and σ_{EA}.

The direct ionization cross sections are first calculated in a configuration average distorted-wave approximation, which is described in detail in the proceedings of a NATO Advanced Study Institute [9]. The configuration average cross sections are resolved as to initial and final LSJ levels by purely algebraic transformations [10]. Experimental threshold energies are then incorporated using a simple energy scaling of the resolved cross sections.

Inner-shell excitation cross sections are calculated in a multi-configuration J level resolved distorted-wave (DW) approximation. For some years we have calculated inner-shell excitation cross sections using an LSJ level resolved collisional excitation code [11] based on Cowan's HFR atomic structure program [12]. For this project the LSJ resolved collisional cross sections are calculated using an extensively modified version of the Belfast Iron Project R-Matrix codes [13]. The STG1, STG2, and STGJK codes are used to generate configuration-interaction N-electron bound state wavefunctions, term coupling coefficients, and (N+1)-electron scattering algebra. A code labeled STGDWLS calculates non-unitarized LS distorted-wave cross sections, and a code labeled STGDWIC transforms the LS K-matrices to intermediate coupled cross sections.

The branching ratios for autoionization are calculated in a configuration interaction LSJ level resolved distorted-wave approximation using the AUTOSTRUCTURE code [14,15]. In order to obtain the EA cross sections (Eq. (4)), each excitation cross section (obtained from STGDWIC) is multiplied by the appropriate branching ratio (from AUTOSTRUCTURE). Thus, special care has been taken in order to obtain very close values of the energies by using both codes, for a correct identification of the same level in both programs.

As a completely independent test we used the HULLAC package [16] for the EA calculations. In this package, the atomic structure is calculated by using the fully relativistic, multiconfigurational, RELAC[1] code, based on the parametric potential model citeKlapisch71. The main idea of this approach is the introduction of a central potential as an analytic function of screening parameters which are determined by minimizing the first-order relativistic energy of a set of configurations. An extended version of this code [18] is used to calculate the autoionization and radiative rates needed for branching ratios. The collisional excitation cross sections are calculated in the DW approximation by using the CROSS code. This code uses the factorization-interpolation method [16], which significantly improves the computational efficiency for the calculation of the radial integrals.

For current plasma modeling codes the branching ratios need to be resolved as to the final J level. On the other hand, for comparisons with atomic collision experiments that measure charge-changing events, only branching ratios summed over all final states are required (i.e., $\sum_f B_a(j \to f)$). The J level resolved ionization cross sections are entered into the atomic database in the form of Maxwell-averaged rate coefficients. The numerical entry format is that developed for ADAS [2,19]. Future updates are made easier by separately cataloging rate coefficients for direct ionization and excitation–autoionization.

3. Electron-impact ionization of Fe^{14+}

Our example from the ionization database for the Mg isoelectronic sequence is Fe^{14+}. The Maxwellian rate coefficients for direct ionization of Fe^{14+} (seq='Mg', nucchl=26) are presented in Table 1 for the transitions from the ground level $2s^22p^63s^2$ to the many levels of the configuration $2s^22p^63s$, $2s^22p^53s^2$, and $2s2p^63s^2$, and the transitions from the metastable levels $2s^22p^63s3p$ $^3P_{0,2}$ to the levels of the configuration $2s^22p^63s$, $2s^22p^63p$, and $2s^22p^53s3p$. The initial (nlev) and final (nprf) levels are identified by configuration, spin multiplicity (S), orbital angular momentum (L), and total angular momentum (WJ). The ionization potentials (bwni, bwnf) and level splittings (wni, wnf) are in cm^{-1}. The direct ionization rates in cm^3 sec^{-1} from each

---

[1] Developed by M. Klapisch, A. Bar-Shalom, and E. Luc-Koenig.

Table 1
Maxwellian rate coefficients for direct ionization of Fe^{14+} (file **adf23.ea**)

```
seq ='Mg'    nucch1 =26                                              ADF23

   final level indexing       bwnf =   3946116.3    nprf = 24
   --------------------
   indf   code          S L   WJ       wnf
   ----   ----          - -   --   ------------
      1  2s22p63s13p0   (2)0( 0.5)          0.0
      2  2s22p63s03p1   (2)1( 0.5)     278347.7
      3  2s22p63s03p1   (2)1( 1.5)     299011.5
     27  2s22p53s23p0   (2)1( 1.5)    5772035.8
     28  2s22p53s23p0   (2)1( 0.5)    5873249.5
     29  2s22p53s13p1   (4)0( 1.5)    5948000.4
     30  2s22p53s13p1   (4)2( 2.5)    5975455.3
     31  2s22p53s13p1   (4)2( 3.5)    5980899.5
     32  2s22p53s13p1   (4)2( 1.5)    5982343.2
     33  2s22p53s13p1   (2)1( 0.5)    5996086.8
     34  2s22p53s13p1   (4)1( 2.5)    6007797.9
     35  2s22p53s13p1   (2)2( 1.5)    6008523.8
     36  2s22p53s13p1   (2)0( 0.5)    6034551.1
     37  2s22p53s13p1   (4)2( 0.5)    6071991.0
     38  2s22p53s13p1   (4)2( 1.5)    6083064.9
     39  2s22p53s13p1   (4)1( 0.5)    6092380.5
     40  2s22p53s13p1   (4)1( 1.5)    6096614.9
     41  2s22p53s13p1   (2)2( 2.5)    6103083.4
     42  2s22p53s13p1   (2)2( 2.5)    6117665.8
     43  2s22p53s13p1   (2)1( 1.5)    6133046.7
     44  2s22p53s13p1   (2)1( 0.5)    6203434.1
     45  2s22p53s13p1   (2)2( 1.5)    6222105.7
     46  2s22p53s13p1   (2)0( 0.5)    6278531.8
     47  2s12p63s23p0   (2)0( 0.5)    6907808.5

   initial level indexing    bwni =   3653000.6    nlev =  5
   --------------------
   indi   code          S L   WJ       wni
   ----   ----          - -   --   ------------
      1  2s22p63s23p0   (1)0( 0.0)          0.0
      2  2s22p63s13p1   (3)1( 0.0)     216533.9
      3  2s22p63s13p1   (3)1( 1.0)     222542.7
      4  2s22p63s13p1   (3)1( 2.0)     236544.4
      5  2s22p63s13p1   (1)1( 1.0)     357284.6

---------------------------------------------------------------------------
meti*= 1

   ionis rates
   -----------
   indf Te= 4.50E+05 1.12E+06 2.25E+06 4.50E+06 1.12E+07 2.25E+07 4.50E+07 1.12E+08 2.25E+08 4.50E+08 1.12E+09 2.25E+09
   ---- ---
      1      1.39E-15 2.15E-12 2.65E-11 9.54E-11 2.00E-10 2.40E-10 2.41E-10 2.08E-10 1.73E-10 1.38E-10 9.95E-11 7.63E-11
     27      4.97E-24 5.85E-16 3.21E-13 8.12E-12 6.00E-11 1.17E-10 1.57E-10 1.70E-10 1.57E-10 1.35E-10 1.04E-10 8.23E-11
     28      1.79E-24 2.57E-16 1.50E-13 3.94E-12 2.97E-11 5.84E-11 7.89E-11 8.55E-11 7.91E-11 6.82E-11 5.24E-11 4.15E-11
     47      3.65E-26 3.95E-17 4.58E-14 1.72E-12 1.67E-11 3.64E-11 5.29E-11 6.10E-11 5.82E-11 5.13E-11 4.02E-11 3.23E-11

---------------------------------------------------------------------------
meti*= 2

   ionis rates
   -----------
   indf Te= 4.50E+05 1.12E+06 2.25E+06 4.50E+06 1.12E+07 2.25E+07 4.50E+07 1.12E+08 2.25E+08 4.50E+08 1.12E+09 2.25E+09
   ---- ---
      1      1.93E-15 1.97E-12 2.12E-11 7.02E-11 1.37E-10 1.58E-10 1.55E-10 1.30E-10 1.07E-10 8.52E-11 6.14E-11 4.72E-11
      2      5.68E-16 9.90E-13 1.28E-11 4.68E-11 9.94E-11 1.20E-10 1.21E-10 1.05E-10 8.71E-11 6.98E-11 5.03E-11 3.85E-11
      6      6.30E-25 6.85E-17 3.66E-14 9.15E-13 6.71E-12 1.30E-11 1.75E-11 1.89E-11 1.75E-11 1.50E-11 1.15E-11 9.14E-12
     29      1.41E-24 1.64E-16 8.96E-14 2.26E-12 1.67E-11 3.26E-11 4.38E-11 4.73E-11 4.37E-11 3.77E-11 2.89E-11 2.29E-11
     32      4.05E-25 4.84E-17 2.66E-14 6.76E-13 5.01E-12 9.77E-12 1.31E-11 1.42E-11 1.31E-11 1.13E-11 8.68E-12 6.88E-12
     35      9.72E-25 1.19E-16 6.61E-14 1.68E-12 1.25E-11 2.44E-11 3.29E-11 3.55E-11 3.29E-11 2.83E-11 2.17E-11 1.72E-11
     36      1.79E-25 2.30E-17 1.30E-14 3.34E-13 2.50E-12 4.88E-12 6.58E-12 7.12E-12 6.58E-12 5.67E-12 4.36E-12 3.45E-12
     37      1.06E-24 1.46E-16 8.47E-14 2.20E-12 1.66E-11 3.25E-11 4.39E-11 4.76E-11 4.40E-11 3.79E-11 2.91E-11 2.31E-11
     38      1.02E-24 1.44E-16 8.41E-14 2.20E-12 1.66E-11 3.25E-11 4.39E-11 4.76E-11 4.40E-11 3.80E-11 2.92E-11 2.31E-11
     39      1.98E-25 2.85E-17 1.67E-14 4.38E-13 3.31E-12 6.50E-12 8.79E-12 9.52E-12 8.82E-12 7.60E-12 5.84E-12 4.63E-12
     40      9.76E-25 1.42E-16 8.34E-14 2.19E-12 1.65E-11 3.25E-11 4.39E-11 4.76E-11 4.41E-11 3.80E-11 2.92E-11 2.31E-11
     43      4.34E-26 6.77E-18 4.08E-15 1.08E-13 8.24E-13 1.62E-12 2.20E-12 2.39E-12 2.21E-12 1.91E-12 1.46E-12 1.16E-12
     44      6.92E-26 1.24E-17 7.80E-15 2.12E-13 1.64E-12 3.25E-12 4.41E-12 4.79E-12 4.44E-12 3.83E-12 2.95E-12 2.34E-12
     46      1.63E-25 3.02E-17 1.93E-14 5.27E-13 4.09E-12 8.11E-12 1.10E-11 1.20E-11 1.11E-11 9.60E-12 7.38E-12 5.85E-12
     47      2.72E-26 5.62E-18 3.72E-15 1.04E-13 8.13E-13 1.62E-12 2.21E-12 2.41E-12 2.23E-12 1.93E-12 1.48E-12 1.18E-12
```

Table 1 — continued

```
-------------------------------------------------------------------------------
met i*= 4

   ionis rates
   -----------
   indf Te= 4.50E+05  1.12E+06  2.25E+06  4.50E+06  1.12E+07  2.25E+07  4.50E+07  1.12E+08  2.25E+08  4.50E+08  1.12E+09  2.25E+09
   ---- ---
      1     2.06E-15  2.02E-12  2.14E-11  7.05E-11  1.37E-10  1.58E-10  1.54E-10  1.29E-10  1.06E-10  8.48E-11  6.11E-11  4.70E-11
      3     5.66E-16  9.90E-13  1.28E-11  4.68E-11  9.94E-11  1.20E-10  1.21E-10  1.05E-10  8.71E-11  6.98E-11  5.03E-11  3.86E-11
     29     6.72E-25  7.03E-17  3.71E-14  9.20E-13  6.72E-12  1.30E-11  1.75E-11  1.89E-11  1.74E-11  1.50E-11  1.15E-11  9.12E-12
     30     6.92E-25  7.64E-17  4.10E-14  1.03E-12  7.54E-12  1.47E-11  1.97E-11  2.13E-11  1.96E-11  1.69E-11  1.30E-11  1.03E-11
     31     2.17E-24  2.43E-16  1.31E-13  3.28E-12  2.41E-11  4.69E-11  6.30E-11  6.81E-11  6.29E-11  5.42E-11  4.16E-11  3.29E-11
     32     1.50E-25  1.68E-17  9.07E-15  2.28E-13  1.67E-12  3.26E-12  4.38E-12  4.73E-12  4.37E-12  3.76E-12  2.89E-12  2.29E-12
     33     1.08E-25  1.24E-17  6.74E-15  1.70E-13  1.25E-12  2.44E-12  3.28E-12  3.55E-12  3.28E-12  2.82E-12  2.17E-12  1.72E-12
     34     1.12E-24  1.32E-16  7.23E-14  1.83E-12  1.35E-11  2.64E-11  3.55E-11  3.83E-11  3.54E-11  3.05E-11  2.34E-11  1.86E-11
     35     1.04E-25  1.22E-17  6.69E-15  1.69E-13  1.25E-12  2.44E-12  3.29E-12  3.55E-12  3.28E-12  2.83E-12  2.17E-12  1.72E-12
     36     1.91E-25  2.36E-17  1.32E-14  3.36E-13  2.50E-12  4.88E-12  6.58E-12  7.11E-12  6.58E-12  5.67E-12  4.35E-12  3.45E-12
     37     1.13E-26  1.50E-18  8.57E-16  2.22E-14  1.66E-13  3.25E-13  4.39E-13  4.75E-13  4.40E-13  3.79E-13  2.91E-13  2.31E-13
     38     1.09E-25  1.48E-17  8.52E-15  2.21E-13  1.66E-12  3.25E-12  4.39E-12  4.75E-12  4.40E-12  3.79E-12  2.91E-12  2.31E-12
     39     5.28E-26  7.31E-18  4.23E-15  1.10E-13  8.29E-13  1.63E-12  2.20E-12  2.38E-12  2.20E-12  1.90E-12  1.46E-12  1.15E-12
     40     3.54E-25  4.95E-17  2.87E-14  7.49E-13  5.63E-12  1.11E-11  1.49E-11  1.62E-11  1.50E-11  1.29E-11  9.91E-12  7.86E-12
     41     6.88E-25  9.74E-17  5.68E-14  1.48E-12  1.12E-11  2.20E-11  2.96E-11  3.21E-11  2.97E-11  2.56E-11  1.97E-11  1.56E-11
     42     2.19E-25  3.19E-17  1.87E-14  4.92E-13  3.72E-12  7.32E-12  9.89E-12  1.07E-11  9.92E-12  8.55E-12  6.57E-12  5.21E-12
     43     1.16E-25  1.74E-17  1.03E-14  2.72E-13  2.06E-12  4.06E-12  5.49E-12  5.96E-12  5.52E-12  4.76E-12  3.65E-12  2.90E-12
     44     1.85E-26  3.17E-18  1.97E-15  5.33E-14  4.10E-13  8.12E-13  1.10E-12  1.20E-12  1.11E-12  9.57E-13  7.35E-13  5.83E-13
     45     1.74E-26  3.10E-18  1.95E-15  5.30E-14  4.10E-13  8.11E-13  1.10E-12  1.20E-12  1.11E-12  9.58E-13  7.36E-13  5.84E-13
     46     2.90E-26  5.77E-18  3.77E-15  1.04E-13  8.15E-13  1.62E-12  2.21E-12  2.40E-12  2.23E-12  1.92E-12  1.48E-12  1.17E-12


   C  ---------------------------------------------------------------------------
   C  Data generated by Dario M. Mitnik     on 29/12/97
   C
   C  The rates were calculated using configuration-average ionization cross
   C  sections, with semi-relativistic wavefunctions, using the
   C  frozen-core approximation , the post form  for the scattering
   C  potentials, and the maximum-interference approximation.
   C  They were then multiplied by the appropriate angular coefficients.
   C  ---------------------------------------------------------------------------
```

initial level (indi) to each final level (indf) are tabulated as a function of electron temperature (Te) in Kelvin. The data entry is signed and dated at the bottom with a short description of the theoretical procedure used to generate the atomic data.

Excitation–autoionization cross sections are presented in Fig. 1 for the transitions $2s^22p^63s^2 \rightarrow 2s^22p^53s^23\ell$. There are 194 inner-shell excited levels included in these calculations, belonging to the $2s^22p^53s^23\ell$ configurations, and to the $2s^22p^53s3p^2$ and $2s^22p^53s3p3d$ configurations, which are also included in order to provide additional correlations. The dashed curves are the perturbative-relativistic distorted-wave calculations using the STGDWIC code and the solid curves are fully-relativistic distorted-wave calculations using the HULLAC code. The number of partial waves included is sufficient to guarantee convergence of the cross section. The upper curves are the excitation cross sections, which means that all of the branching ratios have been set to unity, while the lower curves show the EA cross section, in which radiation damping is included. For this moderately charged atomic ion, we find good agreement between the perturbative-relativistic and fully-relativistic calculations. There is a difference in threshold energies in the HULLAC and STGDWIC results on the order of 10 eV, a relative difference of about 1.5%. This discrepancies cannot be attributed to relativistic effects only (which are less than 3 eV for this ion); they are a consequence of the different approximations in the orbital calculations. In other calculations of similar ions [20], we have seen differences of about 5 eV. We have done other energy calculations using Fischer's MCHF atomic structure package [21] with different optimizations for the orbitals. These MCHF threshold energies fall between the HULLAC and STGDWIC results.

Total excitation–autoionization cross sections from the ground level are presented in Fig. 2 together with the direct-ionization (DI) cross sections. The additional inner-shell excitation processes included in these calculations are the transitions from the ground level $2s^22p^63s^2$ $^2S_0$ to the $2s^22p^53s^2n\ell$ ($n = 4, 5, 6$) and $2s2p^63s^2n\ell$ ($n = 3, 4$) levels. There are 366 inner-shell excited levels. All electric-dipole allowed radiative decays are considered, and autoionization processes to the $2s^22p^6n\ell$ Na-like levels are taken into account. The
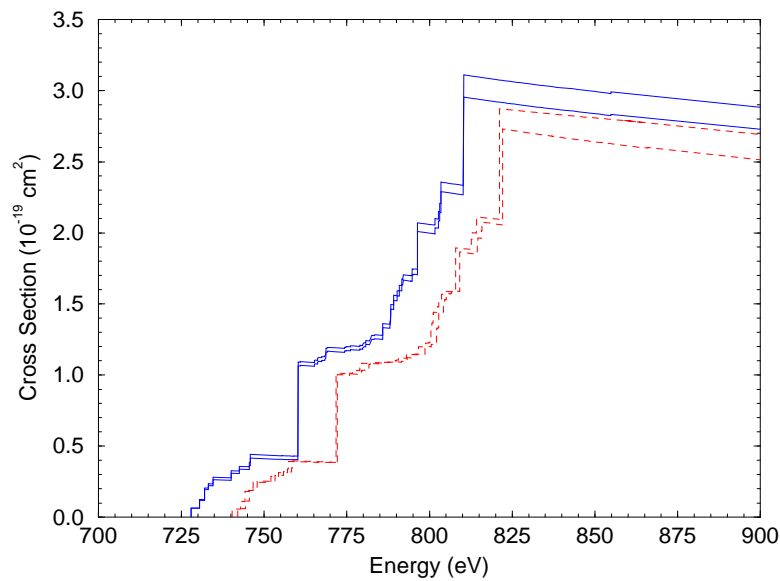
Fig. 1. Excitation–autoionization cross sections from the ground level for Fe^{14+}, including only the $2p \rightarrow 3\ell$ transitions. Upper solid curve: fully-relativistic without radiation damping, lower solid curve: fully-relativistic with radiation damping, upper dashed curve: perturbative-relativistic without radiation damping, lower dashed curve: perturbative-relativistic with radiation damping.
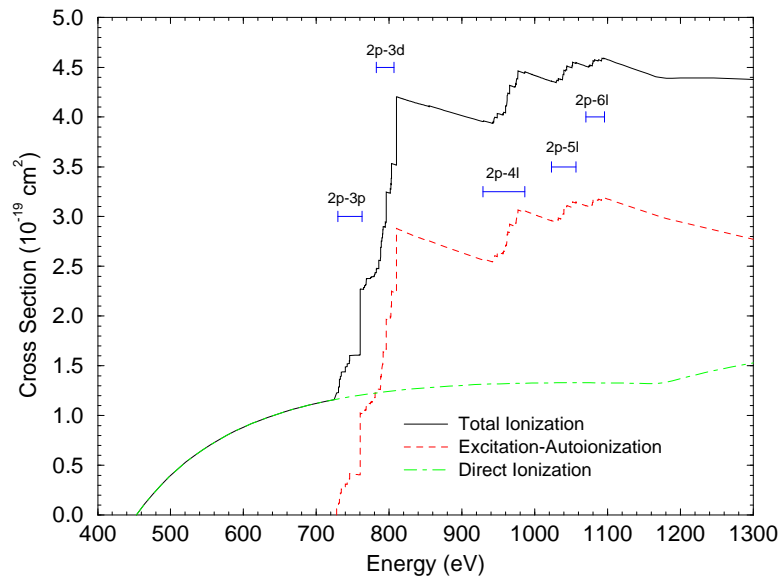

Fig. 2. Total ionization cross sections for Fe^{14+} from the ground level, including the $2p \rightarrow n\ell$ ($n = 3, 4, 5, 6$) and $2s \rightarrow n\ell$ ($n = 3, 4$) transitions. Dashed curve: fully-relativistic EA, dotted-dashed curve: direct ionization, solid curve: total ionization.

dashed curve shows the fully-relativistic distorted-wave calculations for the EA cross section, the dotted-dashed curve the DI cross section, and the solid curve shows the total (EA+DI) ionization cross section. The energy domains of the various inner-shell transitions are indicated above the EA curve.

In Fig. 3 are shown the total ionization cross sections from the metastable levels $2s^2 2p^6 3s 3p$ $^3P_{0,2}$ (dashed curves) together with the total ionization cross section from the ground level. The inner-shell configurations
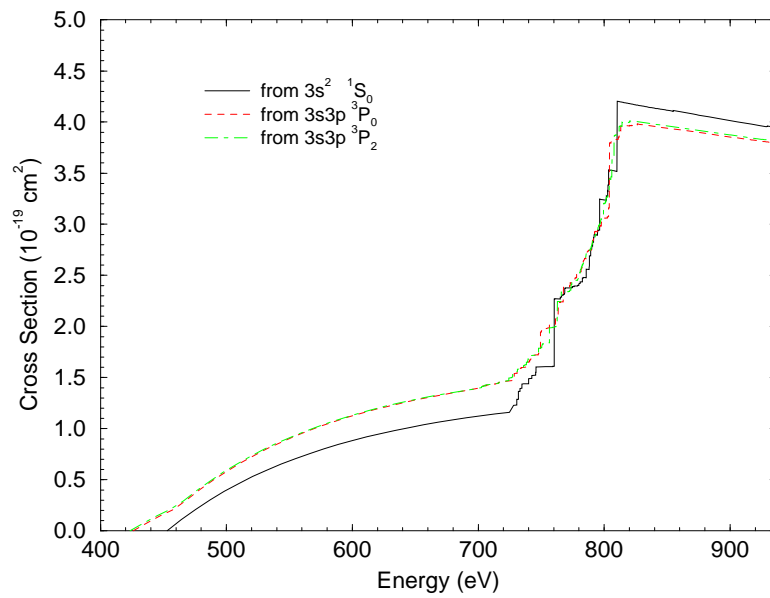
Fig. 3. Total ionization cross sections for Fe^{14+} from the metastable levels $2s^2 2p^6 3s3p \ ^3P_{0,2}$, including the $2p \rightarrow 3\ell$ transitions. Solid curve: total ionization from the ground level, dashed curves: total ionization from the metastable levels.
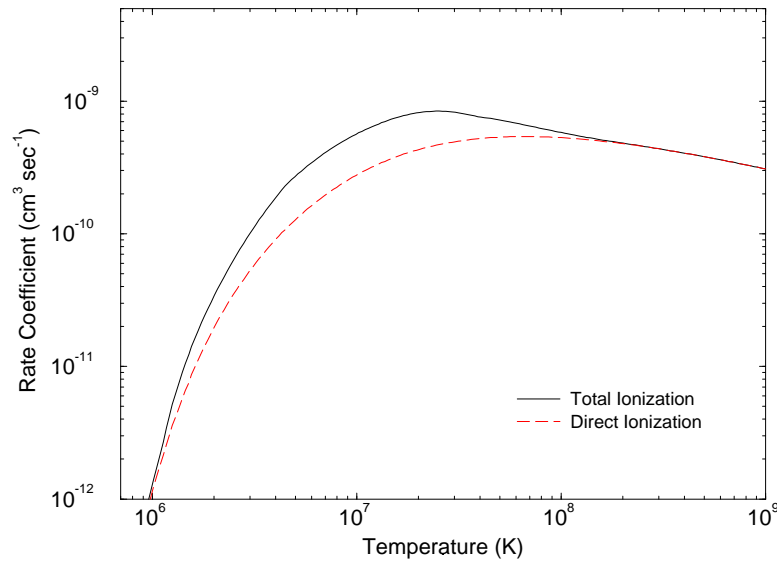

Fig. 4. Maxwellian rate coefficients for Fe^{14+}. Solid curve: total ionization from the ground level, dashed curve: direct ionization only.

included for the calculations from the metastable levels are $2s^2 2p^5 3s3p3\ell$ and $2s^2 2p^5 3s3p4\ell$ (403 levels).

The Maxwellian rate coefficients for indirect ionization, obtained using the radiation-damped cross sections, are presented in Table 2. Finally, we present the Maxwellian rate coefficient for the total electron-impact ionization of Fe^{14+} in Fig. 4. The additional enhancement due to excitation–autoionization is found to be quite substantial over a wide temperature range. In order to emphasize the effect of EA on the ionization balance in plasmas, it is convenient to introduce an effective enhancement factor of the collisional ionization rate coefficient due to the EA processes, defined by [22]

Table 2
Maxwellian rate coefficients for excitation–autoionization of Fe^{14+} (file **adf23.di**)

```
seq ='Mg'    nucch1 =26                                                            ADF23

   final level indexing       bwnf =   3939135.8    nprf = 26
   ---------------------
   indf   code         S L   WJ      wnf
   ----   ----         - -   --   ------------
     1  2s22p63s13p0    (2)0( 0.5)         0.0
     2  2s22p63s03p1    (2)1( 0.5)     278397.7
     3  2s22p63s03p1    (2)1( 1.5)     299071.9
     4  2s22p63s03d1    (2)2( 1.5)     676599.7
     5  2s22p63s03d1    (2)2( 2.5)     679266.7
     6  2s22p63s04s1    (2)0( 0.5)    1865649.6
     7  2s22p63s04p1    (2)1( 0.5)    1975969.4
     8  2s22p63s04p1    (2)1( 1.5)    1984108.0
     9  2s22p63s04d1    (2)2( 1.5)    2122491.2
    10  2s22p63s04d1    (2)2( 2.5)    2123787.0
    11  2s22p63s04f1    (2)3( 2.5)    2182182.2
    12  2s22p63s04f1    (2)3( 3.5)    2182672.8
    13  2s22p63s05s1    (2)0( 0.5)    2660418.8
    14  2s22p63s05p1    (2)1( 0.5)    2714812.2
    15  2s22p63s05p1    (2)1( 1.5)    2718824.8
    16  2s22p63s05d1    (2)2( 1.5)    2785578.8
    17  2s22p63s05d1    (2)2( 2.5)    2786265.2
    18  2s22p63s05f1    (2)3( 2.5)    2815595.2
    19  2s22p63s05f1    (2)3( 3.5)    2815843.8
    20  2s22p63s06s1    (2)0( 0.5)    3072519.8
    21  2s22p63s06p1    (2)1( 0.5)    3103201.8
    22  2s22p63s06p1    (2)1( 1.5)    3105470.2
    23  2s22p63s06d1    (2)2( 1.5)    3142857.8
    24  2s22p63s06d1    (2)2( 2.5)    3143261.8
    25  2s22p63s06f1    (2)3( 2.5)    3160079.2
    26  2s22p63s06f1    (2)3( 3.5)    3160222.8


   initial level indexing    bwni =   3653050.8    nlev =  5
   --------------------
   indi   code         S L   WJ      wni
   ----   ----         - -   --   ------------
     1  2s22p63s23p0    (1)0( 0.0)         0.0
     2  2s22p63s13p1    (3)1( 0.0)     215922.9
     3  2s22p63s13p1    (3)1( 1.0)     221861.0
     4  2s22p63s13p1    (3)1( 2.0)     235619.5
     5  2s22p63s13p1    (1)1( 1.0)     359800.2


-------------------------------------------------------------------------------
meti*= 1

   idion rates
   -----------
   indf Te= 4.50E+05  1.12E+06  2.25E+06  4.50E+06  1.13E+07  2.25E+07  4.50E+07
   ---- ---
     1     1.97E-18  2.33E-13  9.71E-12  5.67E-11  1.41E-10  1.72E-10  9.59E-11
     2     3.98E-19  2.66E-14  8.37E-13  3.90E-12  7.62E-12  8.24E-12  4.13E-12
     3     6.54E-19  5.27E-14  1.74E-12  8.62E-12  1.92E-11  2.37E-11  5.53E-12
     4     3.63E-19  7.11E-14  3.17E-12  1.85E-11  4.61E-11  5.78E-11  1.69E-11
     5     4.58E-19  7.50E-14  3.28E-12  1.87E-11  4.38E-11  5.20E-11  2.10E-11
     6     3.64E-22  4.70E-16  4.12E-14  3.36E-13  1.05E-12  1.51E-12  1.83E-12
     7     1.82E-21  3.43E-15  3.53E-13  3.03E-12  9.16E-12  1.21E-11  1.31E-11
     8     2.14E-21  3.85E-15  3.78E-13  3.05E-12  8.27E-12  1.00E-11  1.02E-11
     9     7.01E-22  1.00E-15  9.32E-14  7.32E-13  1.88E-12  2.16E-12  1.17E-12
    10     1.34E-21  1.97E-15  1.89E-13  1.55E-12  4.48E-12  5.83E-12  2.09E-12
    11     2.44E-22  5.68E-16  6.53E-14  6.01E-13  1.89E-12  2.51E-12  2.32E-12
    12     2.69E-22  6.28E-16  6.93E-14  5.96E-13  1.64E-12  1.94E-12  1.18E-12
    13     1.89E-23  9.53E-17  1.34E-14  1.37E-13  4.84E-13  7.10E-13  8.63E-13
    14     1.63E-22  1.02E-15  1.59E-13  1.70E-12  6.00E-12  8.40E-12  9.45E-12
    15     2.00E-22  1.17E-15  1.75E-13  1.79E-12  5.90E-12  7.89E-12  8.57E-12
    16     4.60E-23  2.43E-16  3.37E-14  3.17E-13  8.60E-13  9.27E-13  7.85E-13
    17     8.13E-23  4.21E-16  5.76E-14  5.30E-13  1.39E-12  1.45E-12  1.19E-12
    18     2.83E-23  1.85E-16  2.83E-14  2.96E-13  1.02E-12  1.40E-12  1.52E-12
    19     3.19E-23  2.05E-16  2.92E-14  2.71E-13  7.35E-13  8.38E-13  7.89E-13
    20     2.98E-24  3.11E-17  5.45E-15  5.99E-14  2.04E-13  2.81E-13  3.22E-13
    21     3.19E-23  3.73E-16  7.14E-14  8.46E-13  3.15E-12  4.48E-12  5.06E-12
    22     4.16E-23  4.57E-16  8.43E-14  9.66E-13  3.43E-12  4.73E-12  5.23E-12
    23     8.63E-24  9.17E-17  1.62E-14  1.73E-13  5.12E-13  5.74E-13  4.99E-13
    24     1.53E-23  1.57E-16  2.71E-14  2.82E-13  8.03E-13  8.68E-13  7.28E-13
    25     7.01E-24  8.31E-17  1.54E-14  1.76E-13  6.33E-13  8.79E-13  9.60E-13
    26     7.88E-24  9.17E-17  1.59E-14  1.63E-13  4.70E-13  5.46E-13  5.18E-13
```

Table 2 — continued

```
-------------------------------------------------------------------------------
met i*= 2

   idion rates
   -----------
 indf Te= 4.50E+05  1.12E+06  2.25E+06  4.50E+06  1.13E+07  2.25E+07  4.50E+07
 ---- ---
     1     3.29E-14  3.14E-13  1.36E-11  8.11E-11  2.11E-10  2.71E-10  2.93E-10
     2     1.06E-14  9.55E-14  3.74E-12  2.03E-11  4.57E-11  5.22E-11  5.01E-11
     3     4.72E-15  4.11E-14  1.53E-12  7.75E-12  1.56E-11  1.67E-11  1.56E-11
     4     2.38E-15  2.21E-14  9.15E-13  5.04E-12  1.19E-11  1.46E-11  1.56E-11
     5     1.07E-15  9.50E-15  3.63E-13  1.74E-12  3.06E-12  2.86E-12  2.34E-12
     6     7.43E-17  1.20E-15  1.26E-13  1.15E-12  3.89E-12  5.56E-12  6.42E-12
     7     1.13E-16  1.90E-15  2.10E-13  1.96E-12  6.61E-12  9.35E-12  1.07E-11
     8     5.55E-17  8.46E-16  7.99E-14  5.96E-13  1.33E-12  1.31E-12  1.07E-12
     9     3.61E-17  5.42E-16  5.00E-14  3.89E-13  9.80E-13  1.06E-12  9.24E-13
    10     4.18E-17  6.20E-16  5.58E-14  4.24E-13  1.04E-12  1.13E-12  1.02E-12
    11     1.55E-17  2.53E-16  2.69E-14  2.29E-13  6.71E-13  8.60E-13  8.94E-13
    12     1.36E-17  2.18E-16  2.25E-14  1.84E-13  5.06E-13  6.19E-13  6.22E-13

-------------------------------------------------------------------------------
met i*= 4

   idion rates
   -----------
 indf Te= 4.50E+05  1.12E+06  2.25E+06  4.50E+06  1.13E+07  2.25E+07  4.50E+07
 ---- ---
     1     3.10E-14  2.94E-13  1.26E-11  7.47E-11  1.91E-10  2.44E-10  2.61E-10
     2     2.83E-15  2.51E-14  9.56E-13  4.93E-12  1.03E-11  1.15E-11  1.12E-11
     3     1.28E-14  1.16E-13  4.57E-12  2.50E-11  5.68E-11  6.56E-11  6.40E-11
     4     1.44E-15  1.39E-14  6.20E-13  3.67E-12  9.51E-12  1.24E-11  1.37E-11
     5     2.94E-15  2.88E-14  1.30E-12  7.80E-12  2.06E-11  2.71E-11  3.02E-11
     6     2.82E-17  4.41E-16  4.36E-14  3.71E-13  1.14E-12  1.55E-12  1.75E-12
     7     5.39E-17  8.69E-16  9.02E-14  7.79E-13  2.36E-12  3.10E-12  3.38E-12
     8     9.72E-17  1.53E-15  1.52E-13  1.24E-12  3.39E-12  4.14E-12  4.25E-12
     9     1.82E-17  2.71E-16  2.46E-14  1.86E-13  4.44E-13  4.67E-13  4.02E-13
    10     5.99E-17  8.94E-16  8.15E-14  6.27E-13  1.55E-12  1.67E-12  1.45E-12
    11     1.53E-17  2.51E-16  2.65E-14  2.28E-13  6.77E-13  8.79E-13  9.21E-13
    12     2.44E-17  3.90E-16  4.00E-14  3.30E-13  9.23E-13  1.15E-12  1.16E-12

C-------------------------------------------------------------------------------
C
C  Data generated by Dario M. Mitnik  on 26-Nov-97
C
C  The rates were calculated using the HULLAC code
C  This code uses atomic many-electron relativistic wave
C  functions. For the Distorted-Wave collisional excitation
C  cross-sections, the Factorization-Interpolation method
C  is used.
C
C
C  The following intermediate inner-shell excited
C  configurations were included in the calculation:
C
C              2s22p53s23p1 2s22p53s23d1
C   2s22p53s24s1 2s22p53s24p1 2s22p53s24d1 2s22p53s24f1
C   2s22p53s25s1 2s22p53s25p1 2s22p53s25d1 2s22p53s25f1 2s22p53s25g1
C   2s22p53s26s1 2s22p53s26p1 2s22p53s26d1 2s22p53s26f1 2s22p53s26g1 2s22p53s26h1
C              2s12p63s23p1 2s12p63s23d1
C   2s12p63s24s1 2s12p63s24p1 2s12p63s24d1 2s12p63s24f1
C              2s22p53s13p2    2s22p53s13p13d1
C   2s22p53s13p14s1 2s22p53s13p14p1 2s22p53s13p14d1 2s22p53s13p14f1
C-------------------------------------------------------------------------------
C
```

$$R^{\mathrm{EA}} \equiv \frac{S + S^{\mathrm{EA}}}{S}, \tag{6}$$

where S is the direct ionization rate coefficient, and S^{EA} is the EA rate coefficient. The ionization enhancement factor R^{EA} reaches a maximum value of about 2.25 at a temperature of about 3.5×10^6 K, and has values close to 2 for temperatures in the range between 3×10^6 K and 1×10^7 K.

4. Summary

Electron-impact ionization rate coefficients have been calculated in the distorted-wave approximation for transition metal ions in the Mg isoelectronic sequence. A database consisting of two parts has been assembled: (1) direct ionization rate coefficients and (2) indirect ionization rate coefficients. The two parts can be easily combined to yield total ionization rate coefficients resolved as to the final ionized level. Examples of the various database formats have been given for the electron ionization of Fe^{14+}. The complete database in electronic form will reside at the Controlled Fusion Atomic Data Center at Oak Ridge National Laboratory in the USA (http://www-cfadc.phy.ornl.gov/data_and_codes/).

Acknowledgements

References

[1] D.L. Moores, K.J. Reed, Adv. Atm. Mol. Opt. Phys 34 (1994) 301.
[2] M.S. Pindzola, D.C. Griffin, C. Bottcher, Phys. Rev. A 33 (1986) 3787.
[3] S.S. Tayal, R.J.W. Henry, Phys. Rev. A 33 (1986) 3825.
[4] D.C. Griffin, M.S. Pindzola, J. Phys. B 21 (1988) 3253.
[5] M.H. Chen, K.J. Reed, Phys. Rev. A 47 (1993) 1874.
[6] A.M. Howald, D.C. Gregory, F.W. Meyer, R.A. Phaneuf, A. Muller, N. Djuric, G.H. Dunn, Phys. Rev. A 33 (1986) 3779.
[7] H.P. Summers, Adv. Atm. Mol. Opt. Phys. 33 (1993) 275.
[8] M.S. Pindzola, D.C. Griffin, C. Bottcher, S.M. Younger, H.T. Hunter, Nucl. Fusion Suppl. 1 (1987) 21.
[9] M.S. Pindzola, D.C. Griffin, C. Bottcher, in: Atomic Processes in Electron–Ion and Ion–Ion Collisions, F. Brouillard, ed., NATO ASI B 145 (1986) 75.
[10] D.H. Sampson, Phys. Rev. A 34 (1986) 986.
[11] D.C. Griffin, M.S. Pindzola, C. Bottcher, Phys. Rev. A 36 (1987) 3642.
[12] R.D. Cowan, The Theory of Atomic Structure and Spectra (Univ. California Press, 1981);
     RCN,RCN2,RCG and RCE atomic structure programs are available at `ftp://t4.lanl.gov/pub/cowan`.
[13] K.A. Berrington, W.P. Eissner, P.H. Norrington, Comput. Phys. Commun. 92 (1995) 290.
[14] W. Eissner, M. Jones, H. Nussbaumer, Comput. Phys. Commun. 8 (1974) 270.
[15] N.R. Badnell, J. Phys. B 19 (1986) 3827;
     available at CCP2 Virtual Library, `http://patiala.phys.strath.ac.uk/iq/prog.html`.
[16] A. Bar-Shalom, M. Klapisch, J. Oreg, Phys. Rev. A 38 (1988) 1773.
[17] M. Klapisch, Comput. Phys. Commun. 2 (1971) 239.
[18] J. Oreg, W.H. Goldstein, M. Klapisch, A. Bar-Shalom, Phys. Rev. A 44 (1991) 1750.
[19] M.S. Pindzola, D.C. Griffin, N.R. Badnell, H.P. Summers, Nucl. Fusion Suppl. 6 (1996) 117.
[20] M.S. Pindzola, D.M. Mitnik, J.A. Shaw, D.C. Griffin, N.R. Badnell, H.P. Summers, D.R. Shultz, Phys. Scripta 57 (1008) 514.
[21] C.F. Fischer, Comput. Phys. Commun. 64 (1991) 369.
[22] D. Mitnik, P. Mandelbaum, J.L. Schwob, J. Oreg, A. Bar-Shalom, W.H. Goldstein, Phys. Rev. A 50 (1994) 4911.